



Utilizing thiol-ene chemistry to explore the effect of network architecture on the properties of self-healing elastomers

Kory Schimmelfennig^a, Vincent Mei^b, Christopher L. Lewis^{c,*}

^a Rochester Institute of Technology, Department of Chemical Engineering, Rochester, NY, USA

^b Rochester Institute of Technology, Department of Mechanical Engineering, Rochester, NY, USA

^c Rochester Institute of Technology, Department of Manufacturing and Mechanical Engineering Technology, Rochester, NY, USA

ARTICLE INFO

Keywords:

Self-healing
Covalent adaptable networks
Thiol-ene chemistry
Hindered urea bonds
Rubber elasticity
Network structure

ABSTRACT

Dynamic covalent chemistry provides the functional basis for the efficient and reliable exchange of reversible binding groups which enable self-repair thus avoiding structural impairment or permanent damage of material properties. Hindered urea bonds (HUBs) have proven easy to incorporate into polymers and exhibit moderate temperature thermo-reversibility and creep resistance. In this investigation we study the effects of preparing covalent adaptable networks (CANs) bearing HUBs using thiol-ene chemistry. A novel poly(urea urethane) prepolymer (PUUP) with di-acrylate functionality was developed and incorporated into networks with thiol building blocks at different stoichiometries; the di-acrylate functionality enables the formation of networks using either photo-initiator or base catalyst. By preparing six distinct networks with various molecular weight per elastically effective network chain (M_c), three photolytically and three base catalyzed, this work aims to elucidate the interdependencies of network topology, mechanical properties, and self-healing resulting from these two synthetic strategies. Dynamic mechanical analysis (DMA) was utilized to measure the modulus of prepared networks, which enabled an assessment of crosslink density. Mechanical testing was then employed to investigate the bulk and self-healing properties of these networks. A wide range of mechanical behavior was exhibited, depending on the preparation strategy: for photo-polymerized networks, elongation at break (ϵ_{max}) ranged from 88 to 152 % and toughness values (U_T) ranged from 0.45 to 0.62 MJ/m³. On the other hand, base catalyzed networks exhibited elongation to break as high as 904 %, and toughness as high as 2.75 MJ/m³. A high healing efficiency of 100 % recovery of toughness (η_U) was exhibited by the base catalyzed sample with highest M_c , whereas photopolymerized networks exhibited significantly reduced performance ($\eta_U = 29$ %). The reduced performance of photopolymerized networks is attributed to a competition between the desirable thiol-ene reaction and the competing free radical polymerization of acrylate groups.

1. Introduction

The preparation of sustainable materials that imitate the recuperative nature of biological organisms has become of central interest to materials scientists and engineers alike over the past few decades. Self-healing materials aim to address the pitfalls associated with aesthetic, minor, corrosive, or even catastrophic damage of polymers, reducing the need to replace polymeric products as often which results in hundreds of billions of dollars lost every year [1]. In particular, self-healing elastomers have been extensively studied for their application in areas such as 3D printing [2,3,4,5], conductive devices [6], sensors [7,8], soft robotics [9,10], surface protective coatings [11], and biomedical engineering

[12]. This work aims to help elucidate the relationship between the manner in which the elastomer is made and the resulting properties, establishing fitness for use in these applications. Seeking to prepare reprocessable and recyclable materials with comparable mechanical properties, invariance to creep, solvent and abrasion resistance, and the load-bearing capacity of thermosets, scientists have explored developing covalent adaptable networks (CANs) [13,14]. By introducing plasticity at or between junctions of crosslinked networks, the efficient and reliable exchange of reversible binding groups enables self-repair thus avoiding structural impairment or permanent damage of material properties [13,14,15]. Reversible binding groups such as hindered urea bonds (HUBs) have provided the functional platform for intrinsically

* Corresponding author.

E-mail address: cllmet@rit.edu (C.L. Lewis).

<https://doi.org/10.1016/j.eurpolymj.2025.113736>

Received 24 October 2024; Received in revised form 19 December 2024; Accepted 9 January 2025

Available online 10 January 2025

0014-3057/© 2025 The Authors. Published by Elsevier Ltd. This is an open access article under the CC BY-NC-ND license (<http://creativecommons.org/licenses/by-nc-nd/4.0/>).

healable polymer systems capable of mending cracks at mild temperatures [15].

This investigation focuses on the relevance of reaction mechanism in preparing CANs via thiol-ene chemistry. Thiol-Michael addition has proven to be well-suited for numerous emerging technologies [16], providing avenues for new research that allow for easier access to more complex functional polymers [16,17,18]. The incorporation of thiols into polymers bearing other stimulus-responsive moieties is an emerging technique for the preparation of multi-functional materials [19], and although the thiol-ene click reaction has been known for over 100 years [20], it has recently regained traction given its applicability to synthetic procedures, and specifically for network synthesis [21].

The mechanical and thermomechanical properties of CANs are primarily governed by the integrated dynamic moiety and form of crosslinking present where finding the balance between self-healability, stretchability, and toughness has proven to be a formidable challenge [6,11,22]. Furthermore, not many systematic works explore the relationship between crosslink density, T_g , and healing efficiency [23]. To address some of these factors, this work relies on the reaction of α,β -unsaturated esters (acrylates) with thiols to prepare CANs. We investigate the differences and benefits of preparing networks using both radical mediated (RM) and base catalyzed (BC) thiol-Michael additions. By forming networks via either photo-initiation or with base catalyst, differences in the architecture of these networks and their concomitant effects on self-healing, can be more closely assessed.

A novel poly(urea urethane) prepolymer (PUUP) bearing dynamic HUBs was prepared and integrated into networks crosslinked via a tri-functional thiol; to the best of our knowledge, this is the first reported example of thiol-ene networks bearing HUBs. In this work, the crosslink density was altered in conjunction with reaction mechanism to aid in developing a more concrete understanding of the relationships between T_g , diffusion characteristics, network topology, as well as mechanical and thermomechanical properties. The molecular weight per elastically effective network chain (M_C) of prepared networks was varied by incorporating a di-functional thiol chain extender at various stoichiometric ratios. The role of polymerization mechanism, radical mediated (RM) or base catalyzed (BC), and stoichiometric feed ratios on the thermal, mechanical, and self-healing performance will be examined. This work aims to elucidate the role of kinetic pathway in striking a balance between the self-healability and mechanical properties of CANs.

2. Materials and methods

2.1. Materials and reagents

Synthesis was completed using as-received materials unless stated otherwise. Dichloromethane (DCM), containing 40–150 ppm amylenes as stabilizer was obtained from Sigma-Aldrich in a minimum of 99.5 % purity. 2,2'-(Ethylenedioxy)diethanethiol (EDODET) and Tetrahydrofuran (anhydrous, THF), both inhibitor-free, were received from Sigma-Aldrich in a minimum of 95 % and 99.9 % purity, respectively. Trimethylolpropane Tris(3-mercaptopropionate) (Tmpt3) was received from Fisher Scientific (>85 % purity). Isophorone diisocyanate (IPDI), a mixture of cis- and trans- isomers, was obtained from Sigma-Aldrich in a minimum of 98 % purity. Poly(tetrahydrofuran) (PTMEG), average M_n ~1000 g/mol, was obtained from Sigma-Aldrich with MQ 200 quality specification, and vacuum dried at 100 °C overnight prior to synthesis. Dibutyltin dilaurate (DBTDL) and N,N'-di-*tert*-butylethylenediamine (TBEDA) were obtained from Sigma-Aldrich in a minimum of 95 % and 98 % purity respectively. 2-Isocyanatoethyl acrylate (ICEA), stabilized with BHT, was received from TCI Americas at a minimum of 98 % purity. ACS grade Hexane was obtained from TCI Americas. Phenylbis(2,4,6-trimethylbenzoyl)phosphine oxide (BAPO) was obtained from Sigma Aldrich in powder form at a minimum of 97 % purity. 1,8-Diazabicyclo [5.4.0]undec-7-ene (DBU) was received from Sigma Aldrich at a minimum of 98 % purity. Prior to monomer synthesis, all glassware was

cleaned with acetone and any moisture was removed by drying at 160 °C for a minimum of 3 hr.

2.2. Synthetic procedures

2.2.1. Preparation of poly(urea urethane) prepolymer (PUUP)

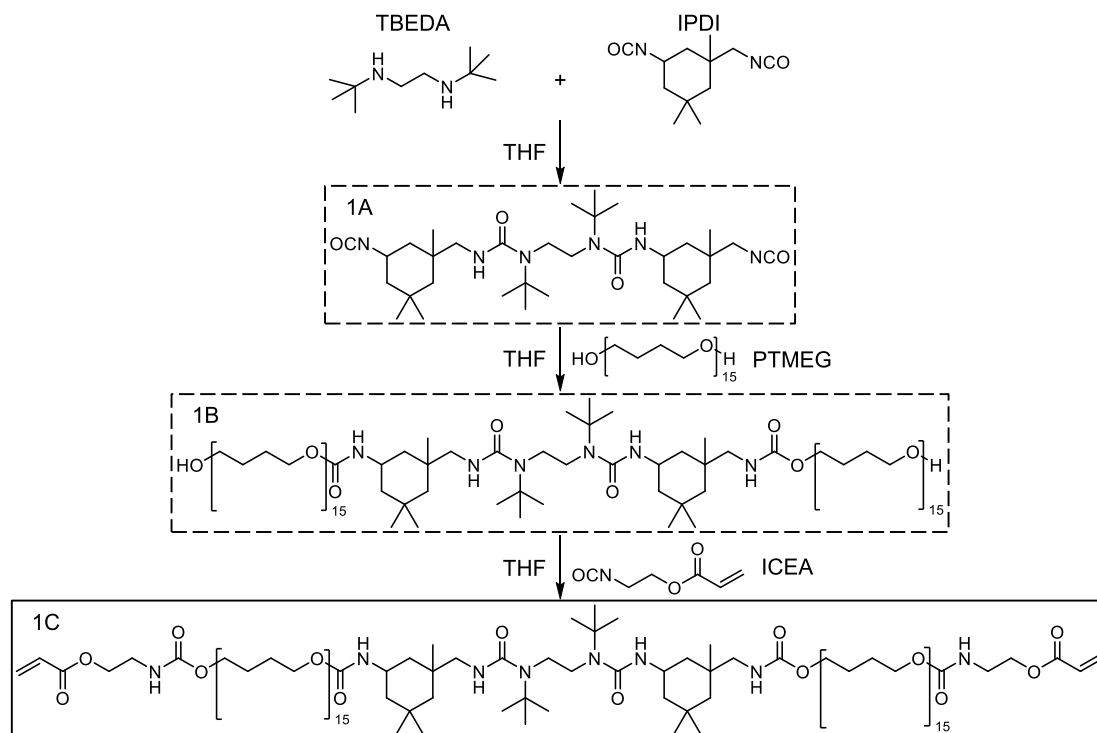
The general synthetic procedure used to prepare the PUUP is shown below in Scheme 1. Here, THF (55 mL) and IPDI (7.43 mL, 35.43 mmol) were added to a 500 mL three-neck round-bottom flask and purged with dry nitrogen, stirring for approximately two minutes. TBEDA (3.82 mL, 17.72 mmol) was added dropwise over a 4–5 min period under vigorous stirring and dried nitrogen flow. The system was then sealed and allowed to stir for 12–15 min. Dried nitrogen flow was reintroduced and additional THF (50 mL) was added. PTMEG (36.38 mL, 35.43 mmol) and 0.6 mol% DBTDL (0.25 mL, 0.43 mmol) were added and the flask was resealed. After stirring for 2 hr, the seal was broken and additional THF (35 mL) was added under dried nitrogen flow. Subsequently, ICEA (4.55 mL, 35.43 mmol) was added dropwise over a 7–9 min time period under vigorous stirring. The flask was then sealed after purging with dried nitrogen and allowed to stir for an additional 2 hr at ambient temperature. Notably, the solution remained transparent for the entirety of the synthetic procedure. Precipitation of the solution in 1600 mL hexane (1X) followed by decanting yielded a viscous, sticky, white colored product (84 % yield). The product was left under dried argon flow for 24 hr; this resulted in a sticky, highly viscous transparent prepolymer as shown in Fig. S1.1.

2.2.2. Preparation of thiol-ene networks

A total of six material formulations were prepared using thiol-ene chemistry; three of these were prepared using a radical mediated (RM) approach and three using a base catalyzed (BC) approach. Additionally, by varying the stoichiometric balance of permanent tri-functional crosslinker (Tmpt3) and di-functional chain extender (EDODET), the molecular weight per elastically effective network chain (M_C) and thus the crosslink density, was varied. Accordingly, these compositions were designated as RM-XX or BC-XX, where XX is replaced by stoichiometric M_C in kg/mol. For example, RM-15 represents a radical mediated thiol-ene sample formulated to obtain an M_C of 15 kg/mol. Conversely, BC-3 represents a base catalyzed thiol-ene sample formulated to obtain an M_C of 3 kg/mol. Table 1 summarizes the prepared formulations.

2.2.2.1. Radical mediated (RM) bulk materials. An appropriate amount of PUUP (~3 g depending on the formulation) was placed into a 20 mL scintillation vial after which DCM (3.2 mL) was added to obtain a solution containing approximately 45 wt% PUUP. This was sealed and allowed to stir until a homogeneous solution was obtained (time ranged 0.5–2 hr). The homogeneous solution was opened and reagents Tmpt3, EDODET (or both depending on formulation) were added, followed by the addition of 1 wt% BAPO. The scintillation vial was sealed with a cap, shielded from light exposure and allowed to stir for an additional 2 hr prior to casting into rectangular glass molds (42 × 45 × 6.4 mm). All radical mediated formulations were cured in an XYZ UV Curing Chamber (UV LED $\lambda = 375$ –405 nm) for 5 min. After polymerization any remaining solvent was removed under dried argon flow for 8 hr followed by vacuum de-gassing for an additional 24 hr. Samples with final thickness of approximately 1.5 mm were de-molded and manually cut into 10 × 20 mm rectangles with a single edge razor blade for mechanical testing.

2.2.2.2. Base catalyzed (BC) bulk materials. The same batch size was used as with radical mediated sample preparation, and a similar procedure was utilized. An appropriate amount of PUUP (~3 g depending on the formulation) was placed into a 20 mL scintillation vial after which DCM (3.2 mL) was added to obtain a solution containing approximately 45 wt% PUUP. This was sealed and allowed to stir until a



Scheme 1. Step-by-step one-pot synthesis of the poly(urea urethane) prepolymer (PUUP).

Table 1
Stoichiometric summary of prepared material formulations.

Formulation	Molar Ratio			Stoichiometric M_c (kg/mol)
	PUUP	TmpT3	EDODET	
RM-3	3	2	0	3.2
RM-15	15	2	12	15.7
RM-30	30	2	27	31.3
BC-3	3	2	0	3.2
BC-6	6	2	3	6.3
BC-12	12	2	9	12.6

homogeneous solution was obtained, anywhere from 0.5 to 2 hr. The homogeneous solution was opened and reagents TmpT3, EDODET (or both depending on formulation) were added, and the solution was sealed and allowed to stir for 0.5–2 hr. DBU (1 mol%) was dissolved in 1 mL DCM and added to the bulk solution, allowed to stir vigorously for 5–15 sec and quickly cast into a rectangular glass mold ($42 \times 45 \times 6.4$ mm). All formulations were allowed to cure for 48 hr in a sealed box. Upon removal from the sealed box, any remaining solvent was removed via 24 hr dried argon flow, then vacuum de-gassing for 24 hr. Samples with final thickness of approximately 1.5 mm were de-molded and post cured for 3 hr at 70°C , then manually cut into 10×20 mm rectangles with a single edge razor blade for mechanical testing.

2.3. Characterization techniques

Fourier Transform Infrared (FTIR) spectroscopy: A PerkinElmer Frontier FTIR with Attenuated Total Reflectance (ATR) attachment (Diamond/ZnSe crystal) was utilized in the $650\text{--}4000\text{ cm}^{-1}$ range, averaging four scans per experiment.

Differential Scanning Calorimetry (DSC): DSC experiments, performed on a TA Instruments DSC2500, were utilized to determine the glass transition temperature (T_g) of prepared thiol-ene networks ($10^\circ\text{C min}^{-1}$, $-90\text{--}130^\circ\text{C}$, 2x loops). Solid polymerized samples, ranging from 5–15 mg were utilized.

Nuclear Magnetic Resonance (NMR): A Bruker BioSpin AG 300

MHz NMR spectrometer was utilized for proton (^1H) NMR characterization; sample concentration in CDCl_3 was approximately 20 ppm.

Gel Permeation Chromatography (GPC): GPC was performed using a Shimadzu LC 2030 plus detector system containing two Agilent ResiPore, 300×7.5 mm columns and a refractive index detector (RI). Experiments were carried out at 1 mL/min (30°C) using HPLC grade chloroform (MilliporeSigma, 99.8 %). Calibration was performed using narrowly distributed polystyrene (PS) supplied by Sigma Aldrich (range = $500\text{--}1,000,000$ g/mol). Sample concentration was 2.5 mg/mL and samples were filtered using a $0.2\ \mu\text{m}$ PTFE filter. A polystyrene analytical standard sample (MilliporeSigma, 70,000 g/mol) was used as a verification standard.

Rheology: Rheological characterization was performed on the PUUP using a TA Instruments DHR2 rheometer over the temperature range $20\text{--}80^\circ\text{C}$, at 20°C increments. Measurements were taken using an 8 mm Peltier plate geometry (1 mm gap) over the frequency range, $\omega = 0.1\text{--}100$ Hz. Strain amplitudes ranging from 0.1–1.5 % were shown to be in the linear viscoelastic region by performing strain sweep experiments ($T = 20^\circ\text{C}$, $\omega = 1$ Hz); as such a strain amplitude of 1 % was selected for these experiments. Resulting curves were analyzed using TRIOS software (TA Instruments).

Dynamic Mechanical Analysis (DMA): DMA was completed on thiol-ene networks using a TA instruments HR20 rheometer with 8 mm cross-hatched upper and lower geometries. 8 mm diameter samples (1.5 mm thickness) were stamped and oscillatory amplitude experiments (1 Hz, 20°C) were completed over the 10^{-4} to 100 % strain range. Strain amplitudes ranging from 0.01–0.1 % were shown to be in the linear viscoelastic region for all formulations. Accordingly, presented values for shear storage modulus (G') were collected at 0.06 % strain. Characteristic DMA curves for each formulation are shown in Fig. SI.2.

Density Measurements: An Ohaus PA114 PioneerTM Analytical Balance (110 g capacity, 0.0001 g readability) was employed with an Ohaus Density Determination Kit. Measurements of all polymerized formulations were taken in triplicate at room temperature in de-ionized water.

Mechanical Testing and Self-healing: An Instron 5567 tensile testing apparatus equipped with a 2525 Series Drop-Through Static 1kN

Load Cell (2525–806) and pneumatic grips, set at 20 psi, were used for this investigation. Bluehill Universal (v4.07) software was used to control the frame and collect data. Rectangular samples ($1.5 \times 10 \times 20$ mm, 8 mm gage length) were uniaxially pulled at 10 mm min^{-1} until complete fracture. Healed specimens were obtained by cutting rectangular samples in half with a single edge razor blade, immediately recombining both halves, and heating at $70 \text{ }^\circ\text{C}$ for 3 hr. At least three pristine and three healed specimens were tested for each formulation. Healing efficiencies were determined with the following equation:

$$\eta_X(\%) = \frac{X_{\max}^{\text{healed}}}{X_{\max}^{\text{pristine}}} * 100 \quad (1)$$

Where X can be replaced by the property that healing efficiency is being evaluated based upon; for example, η_e represents healing efficiency based upon elongation to break.

3. Results and discussion

3.1. Design and characterization of the poly(urea urethane) prepolymer (PUUP)

To systematically explore the relationship between crosslink density, T_g , and healing efficiency, a versatile dynamic crosslinker, the poly(urea urethane) prepolymer (PUUP, Scheme 1) was synthesized; this enabled the preparation of networks via both base catalysis (BC) and radical mediated (RM) thiol-ene reactions owing to its di-acrylate functionality. The selection of TBEDA as the hindered amine was motivated by Ying et al. [15] who demonstrated that resulting HUBs based on this chemistry exhibited a good combination of moderate temperature thermo-reversibility and creep resistance. Moreover, IPDI has gained recent traction as a key component for the development of tough elastomeric materials [6,22] and therefore was chosen for this application. Each isocyanate group of IPDI provides an asymmetric reactive center derivative of the mixture of cis- and trans- isomers [24]; these chiral characteristics enable multiple final conformations thus reducing the probability for chain stacking and this improves both the prepolymer's amorphous character and its solubility in various monomers and solvents. Incorporating IPDI into polymers also provides resistance to abrasion and degradation from ultraviolet light [14,24] and has been shown to reduce relaxation time (τ_d) resulting in self-healing on considerably shorter timescales [25]. Moieties peripheral to central hindered urea bonds (HUBs) have been shown to affect diffusion characteristics [6,15], therefore PTMEG chains were also incorporated into the molecular design as they provide increased flexibility. PTMEG is commercially available at various molecular weights which allows for a facile method to tune molecular weight, though in this study we constrained our investigation to one particular PTMEG molecular weight. ICEA was incorporated into the structure to provide di-acrylate functionality; this enables multiple reaction pathways to form networks including traditional free radical polymerization, the use of thiol-ene chemistry, and aza-Michael addition.

FTIR and ^1H NMR were used to track the progress of the multi-step PUUP reaction. FTIR-ATR curves obtained at each step of the synthetic procedure (Scheme 1) are shown in Fig. 1.

As shown in Scheme 1, the click reaction of TBEDA and IPDI results in HUB precursor formation (1A in Fig. 1). A reduction in the isocyanate peak (2270 cm^{-1}) to half of its absorption between IPDI and 1A indicates the di-substitution of isocyanate with amine; the corresponding formation of central hindered ureas is shown by the presence of urea carbonyls (1630 cm^{-1}) [26]. ^1H NMR and FTIR results presented by Kim et al. [27] and Lee et al. [28] are in good agreement with our results regarding the formation of product 1A. Two hours after the addition of catalyst DBTDL and PTMEG to the precursor (1A), the absence of an isocyanate peak in conjunction with the appearance of urethane carbonyls (1705 cm^{-1}) indicates that urethane groups have formed peripheral to 1A, resulting

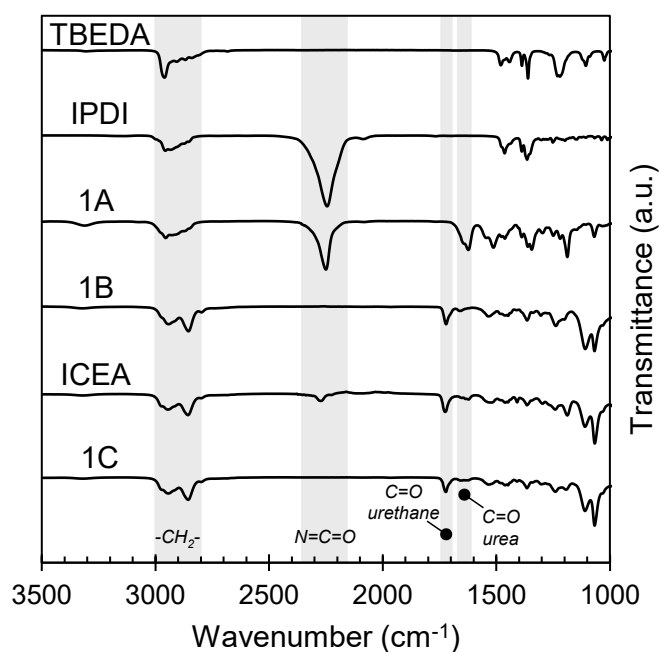


Fig. 1. FTIR-ATR of reactants and intended products during each step of the PUUP synthesis shown in Scheme 1.

in molecule 1B. The PUUP curve (1C) provides evidence that two hours following the influx of ICEA, all isocyanates have been consumed and the urethane groups have formed. ^1H NMR analysis, shown in Fig. SI.3, further corroborates the expected product of synthesis.

In order to determine the molecular weight of the PUUP, GPC and NMR end-group analyses were completed. The predicted molecular weight of the PUUP is 3.1 kg/mol. The average of three GPC runs indicate that the prepared PUUP has an $M_n = 3.3 \text{ kg/mol}$, $M_w = 9.5 \text{ kg/mol}$, and therefore a polydispersity index (PDI) of 2.9. There is good agreement between the PUUP M_n determined via NMR end-group analysis and GPC, as shown in Fig. SI.4, Table SI.1, and Fig. SI.5; the feed ratio for our polymer formulations is based on an $M_n = 2.9 \text{ kg/mol}$, as determined by NMR end-group analysis.

The PUUP monomer is a high viscosity prepolymer owing to the moderately high molecular weight and hydrogen bonding between urea and urethane groups. Viscosity was quantified using rheological characterization via frequency sweeps at 20, 40, 60, and $80 \text{ }^\circ\text{C}$, as provided in Fig. SI.6. At 20 and $40 \text{ }^\circ\text{C}$, the loss modulus is the dominant response variable at low frequency. The crossover of loss (G'') and storage (G') modulus, shown in Fig. SI.6A, indicates a more solid-like response at elevated frequencies and this is likely due to the reversible nature of the HUBs as well as the presence of hydrogen bonding between ureas and urethanes as previously noted. At 60 and $80 \text{ }^\circ\text{C}$, loss modulus (G'') was the dominant response variable over the range of frequencies tested. These results, shown in Fig. SI.6B, indicate the low T_g character of the prepolymer.

3.2. Investigation of PUUP-containing thiol-ene Networks: T_g

When incorporating the PUUP into various networks, transparent elastomeric materials are obtained as shown in Fig. SI.7. The amorphous character of these networks is supported by the presence of a single glass transition (T_g) in DSC curves, as shown in Fig. SI.8; furthermore, neither crystallization nor melting were observed upon cooling and heating, respectively. Differences in network architecture, owing to reaction mechanism and composition, are apparent from the DSC results presented in Fig. 2 below. A strong linear decrease in T_g is observed with increasing M_C for BC networks. Moreover, the BC materials exhibit a reduced T_g as compared to RM materials suggesting that the motion of

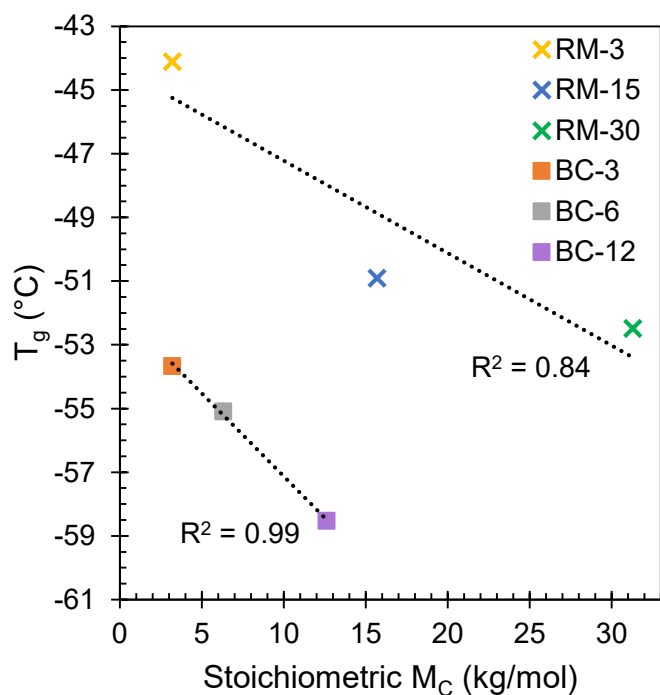


Fig. 2. DSC results of all prepared formulations. T_g of BC networks exhibit a strong linear dependence on crosslink density whereas the linearity of this relationship fails for RM networks.

side chains have an earlier onset for BC networks. In contrast, RM networks exhibit a reduced R^2 value in comparison to BC networks.

The linear dependence of T_g on crosslink density was derived by Fox and Loshaek [29]; the high linearity of T_g for BC formulations fits well with these predictions ($R^2 = 0.99$), noting that the linearity of this relationship is assumed to fail at higher crosslink densities [30]. It is also well known that the presence of crosslinks results in an increase in T_g due to a reduction in free volume.

3.3. Investigation of PUUP-containing thiol-ene Networks: M_C

The predictable reduction in T_g is also apparent when measuring the moduli of these networks using DMA. The dynamic mechanical behavior of these materials can help to explain the complex interaction between network topology and the diffusion characteristics of junctions, chains, and stickers by quantifying the macroscopic effects of elastic free energy associated with chain motion. In particular, the shear storage modulus (G') can be used to estimate the M_C of these networks via the following relation [31,32]:

$$M_C = \frac{\rho}{G'}RT \quad (2)$$

Where ρ is polymer density, G' is shear storage modulus, R is the universal gas constant, and T is absolute temperature. This relation is obtained when both affine deformation and small strains are assumed and is identical to the expression for molecular weight between entanglements [33].

Equation (2) provides an empirical basis to compare the molecular weight per elastically effective network chain between networks ascertained via RM and BC mechanisms. Fig. 3 depicts the dynamic mechanical behavior of prepared materials as a function of their stoichiometric and mechanistic differences. We note that stoichiometric M_C refers to the programmed or ideal M_C based on the feed ratios of reagents when preparing networks; on the other hand, measured M_C is determined using Equation (2) in conjunction with measured values of G' and ρ for each formulation. DMA curves of all prepared formulations are provided in Fig. SI.2.

As shown in Fig. 3A, the measured shear storage moduli of BC networks are substantially lower than values ascertained for RM networks; this result is reflected by the higher measured M_C of BC in comparison to RM formulations, as shown in Fig. 3B. In particular, the diagonal dashed line shown in Fig. 3B represents the ideal elastic response, where measured and stoichiometric M_C (M_{C-M} and M_{C-S} , respectively) are identical; if the M_C determined from G' (measured M_C) is above this line, the material is softer than predicted, and vice versa for a measured M_C below the line. For example, the measured M_C of RM-30 is 5.31 kg/mol, while it was stoichiometrically prepared with an M_C of 31.34 kg/mol; this 6x decrease in M_C indicates the formation of a network with a significantly higher crosslink density than intended. Conversely, BC-3

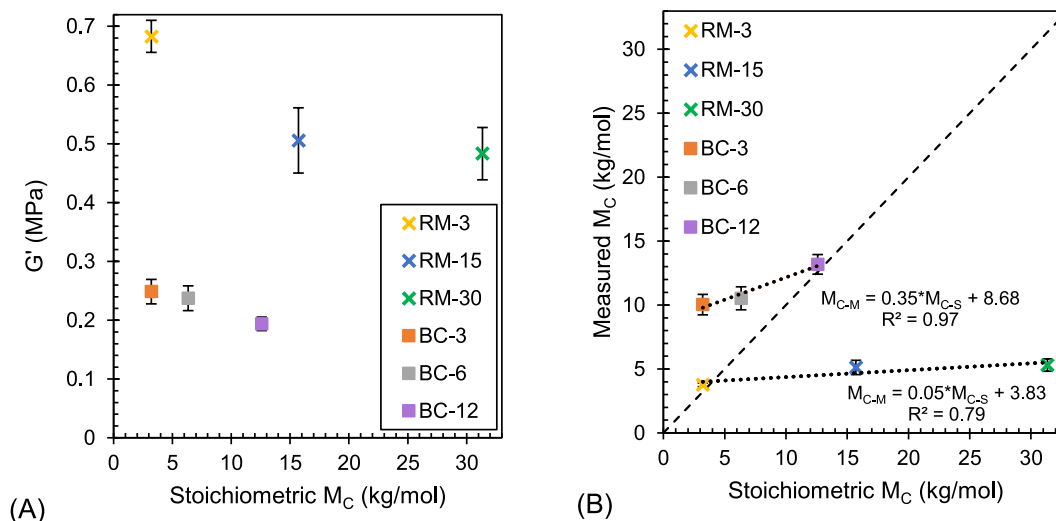


Fig. 3. (A) Effect of M_C and reaction mechanism on shear storage moduli, (B) comparison of measured M_C values (determined via individual measurements of G' and density utilizing Equation (2)) with stoichiometric M_C .

exhibits a measured M_C of 10.04 kg/mol in comparison to its stoichiometric counterpart of just 3.21 kg/mol, indicating an approximate 3x increase in M_C .

Fig. 3B elucidates the differences in stoichiometric and measured M_C by comparing them to an ideal elastic response, as shown by the large diagonal dashed line. Two formulations, RM-3 and BC-12, exhibit elastic responses that are particularly close to the ideal elastic response. The linear trendlines featured in Fig. 3B (small, dotted lines) provide evidence that BC formulations exhibit a more predictable decrease in G' as M_C is increased in comparison to RM formulations; BC and RM formulations exhibit R^2 values of 0.97 and 0.79, respectively. The slope of these trendlines also indicates the vicinity of prepared materials to the proxy for an ideal elastic response (with a slope $m = 1$). The trendline fitted to BC formulations have an $m = 0.35$, whereas RM formulations have an $m = 0.05$. Table 2 presents the percent difference in G' exhibited by all formulations, as well as their measured M_C .

The lowest percent difference in measured versus stoichiometric G' is exhibited by BC-12. The second lowest percent difference is exhibited by RM-3, however, as more chain extender is added to RM formulations their shear storage moduli depart substantially from their predicted values, indicating that RM-15 and RM-30 have much higher concentrations of elastically active crosslinks (EACs) than expected. On the contrary, as more chain extender is added to BC materials, they exhibit lower percent differences in G' . Reconciling these trends is challenging to explain [34], and other investigators have relied on swelling experiments to determine M_C [35,36] or complex imaging tools to pinpoint chain dynamics [36]. Nonetheless, BC formulations exhibit more predictable trends regarding the commensurate decrease in G' with increasing M_C , as well as lower average percent differences in measured versus stoichiometric G' .

The low measured M_C of RM networks presented in Fig. 3 and Table 2 indicate that these formulations have higher concentrations of EACs than BC formulations. A high concentration of EACs in RM networks would result in shorter elastically active network chains. We note that EACs are branching points from which three or more bonds propagate to infinity, acting to terminate elastically active network chains. The crosslink density represents the concentration of elastically active network chains per unit volume.

It is well known that elastically active network chains dictate equilibrium mechanical properties in the rubbery state [37] (i.e., above T_g); it is therefore reasonable to suggest that the higher G' of RM formulations (see Fig. 3A) is the result of shorter elastically active network chains than BC formulations. For example, BC-3 exhibits nearly double the M_C of RM-30 although its stoichiometry should result in an M_C that is approximately 10x lower. This is attributed to anion-mediated step-growth during the formation of BC networks. Step-growth proceeds exponentially, with chain length doubling at every coupling step; as a result, the number of steps required to obtain large chain lengths is small in comparison to reactions that proceed via chain-growth. It is therefore feasible that the networks resulting from base catalysis have a lower concentration of EACs. The PUUP's PDI of 2.9 could also contribute to the low crosslink density of these materials, as this would act to increase the molecular weight between EACs purely from stoichiometric variability. Differences in crosslink density have implications on the mechanical and self-healing properties of these materials, as discussed

later.

The results presented in Table 2 also indicate that there are structural differences between networks prepared via RM and BC mechanisms; radical mediated and base catalyzed polymerization mechanisms (see Fig. SI.9) result in fundamental differences in gel-gel reactions as network structure is built up. Kricheldorf [38] reported that radical mediated polymerizations are more susceptible to chain backbiting as the reaction persists whereas base catalyzed chains typically contain very low percentages of cycles. We suspect that these differences are a result of their kinetics; the radical mediated step-growth reaction between thiol and acrylate results in networks constituted by (intermediary) carbon-centered radicals capable of undergoing both desired chain transfer, but also capable of propagating across another C=C bond which can result in contaminants to the final network structure [20,21]. In general, networks formed in dilute solutions are also subject to an abundance of small cycles [39]; this quality is suspected to be exacerbated during radical mediated network formation owing to coupled chain- and step-growth kinetics. Accordingly, chain-growth of acrylate homopolymerization (depicted in purple, Fig. SI.9A) likely affects final network characteristics of RM formulations [40,41], contrary to BC formulations. While the exact contribution of acrylate homopolymerization cannot be directly determined for RM systems, we highlight differences in prepared networks and their resulting properties. Moreover, traditional free-radical polymerization has more industrial utility than base catalyzed polymerization which would enable the deployment of such material formulations.

For base catalyzed mechanism the proficiency of amine catalyst, overall efficiency of anionic chain process, and a lack of anionic coupling processes that terminate chains once initiated, can result in essentially quantitative yields which proceed at room temperature on the order of minutes or even seconds [20,42]. The selection of DBU as base catalyst was motivated by the positive results obtained by other investigators [16,42], and its ability to convert thiols in the presence of acrylates [21]. Roseli et. al [43] highlight the mechanistic differences between base catalysis and nucleophilic initiation in thiol-Michael additions. The tendency to follow one of these pathways has been explored experimentally and computationally, with notable work providing evidence that the extra driving force attained via reaction of DBU and thiol in ion-pairing solvent dichloromethane tips addition/elimination equilibrium towards base catalysis [43]. The particular importance of this nuanced mechanistic difference is that no by-products are formed when base catalysis occurs [43], as depicted in Fig. SI.9B. These mechanistic differences are supported by the shrinkage of RM formulations by approximately 16% upon polymerization, as compared to the negligible shrinkage observed for BC formulations (see Fig. SI.10 & SI 11). Shrinkage is a symptom of the mixed-mode RM growth mechanism, and results from the development of internal stresses; we found that shrinkage was exhibited by all RM formulations, but not for BC formulations.

3.4. Mechanical properties of PUUP-containing thiol-ene networks

While DMA provides a good proxy for the elasticity of prepared networks, mechanical testing provides a more direct comparison of the rigidity/brittleness of RM and flexibility/ductility of BC formulations.

Table 2
Summary of density and shear storage moduli utilized to determine M_C via Equation (2).

		RM-3	RM-15	RM-30	BC-3	BC-6	BC-12
Measured	ρ_{avg} (kg/m ³)	1052	1054	1048	1020	1021	1046
	G'_{avg} (MPa)	0.68	0.51	0.48	0.25	0.24	0.19
	$M_{C,\text{avg}}$ (kg/mol)	3.76	5.12	5.31	10.04	10.53	13.18
Stoichiometric	G' (MPa)	0.80	0.16	0.08	0.77	0.39	0.20
Difference, G'		-15 %	209 %	493 %	-68 %	-40 %	-4 %

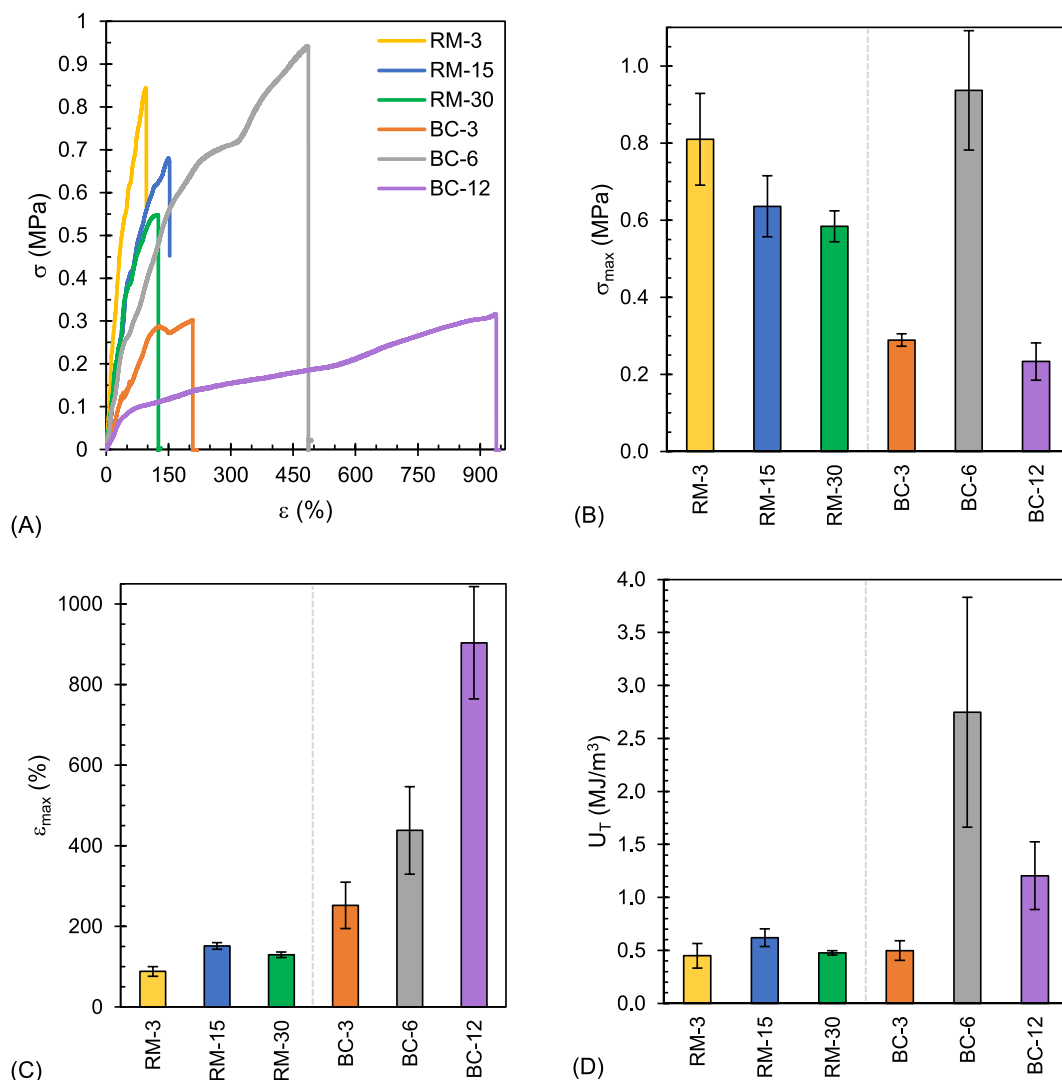


Fig. 4. Summary of (A) characteristic tensile curves, (B) tensile strength at break, (C) elongation at break, and (D) toughness for all prepared thiol-ene networks.

These results are presented in Fig. 4, where a faint dashed gray line divides RM and BC formulations in Fig. 4B-D.

Characteristic tensile curves (Fig. 4A) provide an overview of the differences between mechanical properties of RM and BC formulations as M_C is altered. BC-6 demonstrated the highest maximum tensile strength (σ_{max}) and thus the highest toughness (U_T) of all formulations tested; although it also exhibited the highest standard deviation. The decrease in σ_{max} scales with the increase in measured M_C of RM formulations. Given that the concentration of EACs should decrease as M_C is increased, it would be sensible that the length of elastically active network chains would also increase in a proportionate way. This would be reflected by an increase in the ϵ_{max} of RM formulations complementary to their increase in M_C . This attribute (ϵ_{max}) is a proxy for the elastic activity of chains as they undergo macroscopic deformation. The maximum elongation of all RM formulations is lower than the BC formulation with highest crosslink density (BC-3). Interestingly, ϵ_{max} increases slightly as M_C is increased from 3 kg/mol to 15 kg/mol for RM networks, however, RM-30 exhibits a decrease in ϵ_{max} contrary to what would be expected as M_C increases. One explanation for this trend is the presence of topological defects such as loops in RM formulations given that they exhibit a relative invariance of ϵ_{max} for large increases in M_C .

This may indicate that the free radical homopolymerization of acrylate groups plays a substantial role in the structural development of RM networks, trumping the desirable thiol-ene reaction. Conversely, ϵ_{max} increases substantially in proportion with M_C for BC formulations. This characteristic provides evidence that the elastically active network chains constituting BC networks are more uniformly distributed. We suspect that these trends are derivative of differences in the kinetics of network formation; the step-growth of BC formulations results in the formation of longer chains with fewer defects than the mixed-mode step/chain-growth of RM formulations. As a result, BC networks typically exhibit a delayed gel point in comparison to RM networks [20] thereby increasing the amount of time that chains of BC networks have to obtain preferential conformations before their growth is arrested. This helps to explain the increase in ϵ_{max} of BC-3 in comparison to RM-3, even though they are stoichiometrically equivalent. These results indicate a clear difference in the topological structure of these networks, and in particular, the arrangement of chains within the bulk. The increased slope and quality of fit shown by BC formulations in Fig. 3B would also suggest that these formulations have improved topological uniformity in comparison to RM networks. This is further supported by the low T_g character of BC in comparison to RM formulations (see Fig. 2), which

implies that there are differences in the free volume available for large-scale conformational rearrangements. Ultimately, we attribute the enhanced toughness of BC networks to the kinetic pathway of BC reaction mechanism.

3.5. Self-healing of PUUP-containing thiol-ene networks

With respect to our system, topological-diffusion describes the ability of permanent network junctions (EACs) to diffuse over a limited region of space (i.e., mean position), whether under deformation or thermal stimulus above T_g . In contrast, self-diffusion refers to the motion of dissociated HUB groups under thermal stimulus [44,45]. A natural feature of evaluating self-healing systems is the intimacy of surface-surface contact at the interface to be healed; a time delay may result in chain ends that diffuse into the bulk or undergo chemical reactions and surface rearrangement [46]. The employed healing procedure aims to mitigate this tendency. Healing was performed at 70 °C as temperatures ranging from 60–80 °C are commonly employed for networks containing hindered urea moieties [6,11,22,47]. This temperature is sufficiently high to enable the reversible exchange of hindered urea moieties based on TBEDA. Characteristic overlaid tensile curves of pristine and healed samples are shown in Fig. 5. These three curves are representative of the range of behaviors exhibited by prepared formulations. Overlays for all tested formulations and self-healing efficiencies can be found in Fig. SI.12 and Table SI.2, respectively.

As shown in Fig. 5, the degree of self-healing differs depending on the formulation. Fig. 5A depicts poor retention of toughness, as indicated by the significant reduction in area under the curve of the healed RM-3 sample. Fig. 5B exhibits moderate retention of toughness, where the healed RM-15 sample follows the same curve as the pristine sample back up until failure at a lower ϵ_{\max} . The self-healing efficiency increases substantially as M_C becomes larger, as indicated by the improved retention of toughness (U_T) between RM-3 and RM-15 (Fig. 5A & B). Fig. 5C represents full recovery of toughness, as the healed BC-12 sample follows the same curve as the pristine sample back up until failure at approximately the same ϵ_{\max} . The reported mechanical results do not exceed a coefficient of variation for elongation at break of 26.3 %, putting these results on par with other investigators [6,22,48]. The corresponding self-healing behavior of all formulations is presented in

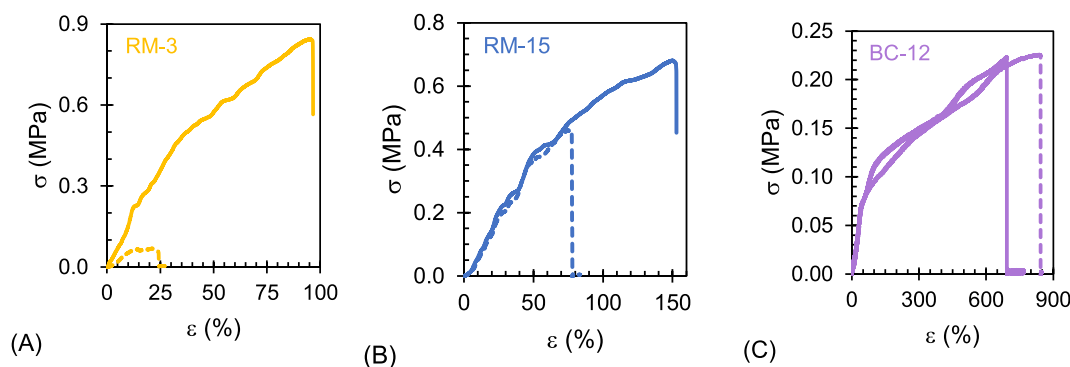


Fig. 5. Characteristic tensile curves of pristine (solid line) and self-healed (dashed line) samples for (A) RM-3, (B) RM-15, and (C) BC-12.

Fig. 6.

The ability of hindered ureas to diffuse a sufficient amount under thermal stimulus is a function of both chain length and the topological uniformity of prepared networks. Moreover, high wettability of the healing interface improves the pace of healing and indicates enhanced chain mobility. A lack of interface wettability was apparent for RM-3, where two of the three healed samples exhibited no significant healing to the point where they were untestable; as such, the single sample that did exhibit only minor healing is shown and therefore no error bars are present (see Fig. 5A and Fig. 6A–C). Just as RM-15 and RM-30 exhibited analogous mechanical properties, these formulations also demonstrated comparable healing characteristics, as shown in Fig. 6A–C. The relative invariance in healing performance and T_g between RM-15 and RM-30, although the M_C is stoichiometrically doubled, suggests that these formulations have poor self-diffusion characteristics. This lack of chain mobility is suspected to be the result of the disorderly structure of RM networks, which impedes the ability of hindered ureas to self-diffuse during healing; another explanation for this behavior are the high measured crosslink densities (i.e., low M_C) of RM-15 and RM-30 as shown in Fig. 3B, which act to restrict the free volume available for self-diffusion during healing. If polymer chains are flanked by a significant number of loops, their physical interaction can provide misleading evidence of the number of EACs and elastically active network chains, as these loops may result in anisotropic deformation under strain. It is therefore suspected that for RM formulations, loops subtend chains as they are stretched, retarding reptation and resulting in networks with a decreased ability to self-heal.

BC-3 exhibited mild healing characteristics and low variability, as shown in Fig. 6D–F. BC-6 demonstrated improved self-healing from BC-3 with higher variability. The most ductile material, BC-12, exhibited exemplar wettability and self-diffusion characteristics as indicated by the tackiness of these materials and high recovery of elongation at break (η_e) following healing. This is attributed to the soft properties of BC-12, which are likely the result of an increase in free volume over other networks examined resulting from the sufficiently high M_C (and low T_g) thus enabling improved diffusion of dissociated HUBs. A summary of the mechanical performance of pristine and healed samples as a function of their average measured M_C is shown in Fig. 7A and B. Recovery based on elongation at break (η_e) is shown in Fig. 7C.

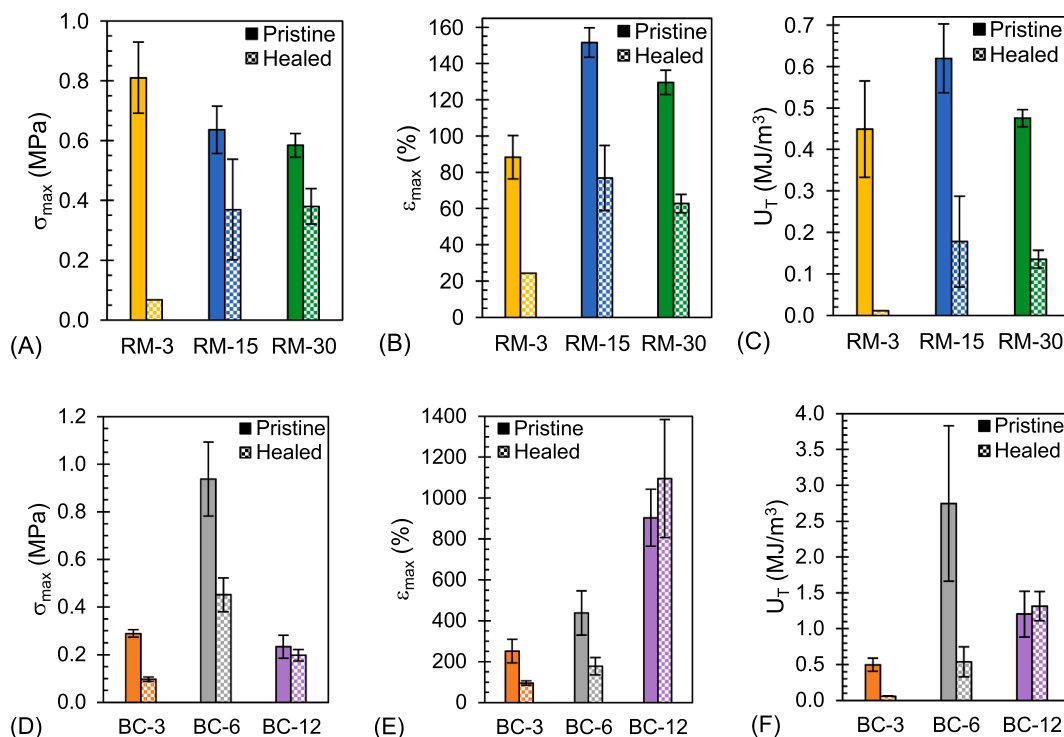


Fig. 6. Comparison of pristine to healed mechanical characteristics for all material formulations. (A) – (C) RM materials, (D) – (F) BC materials.

This study reveals that the mechanical properties of networks prepared using thiol-ene chemistry depend on the employed processing technique. Remarkably, we find that both pristine and healed ϵ_{max} scale proportionally with the average measured M_C . Logarithmic scaling further indicates the magnitude of difference in elongation at break for BC and RM formulations. The improvement in self-healing character appears to be strongly correlated with measured M_C ; as the concentration of EACs decreases, the self-healing performance of these formulations improves. The concentration of HUBs contained between EACs also influences healability; for example, the number of HUBs is stoichiometrically doubled from RM-15 to RM-30 (i.e., ideally RM-15 contains ten HUBs and RM-30 contains twenty HUBs between junctions). For BC formulations, the number of HUBs is stoichiometrically doubled as M_C is increased (i.e., ideally BC-3 contains two HUBs between junctions, BC-6 contains four, and BC-12 contains eight). It is therefore particularly notable that BC-3 and BC-6 exhibit mildly lower self-healing efficiencies than RM-15 and RM-30, given the substantially reduced number of HUBs present in these networks. We suggest that this self-healing performance is due to both the high M_C and topological uniformity of BC networks. Base catalyzed thiol-Michael addition has been shown to produce more ordered network topologies owing to the presence of a temporary thiol adduct which protects C=C bonds during polymerization [49]. This corroborates the importance of both chain dynamics and topological uniformity in facilitating self-healing, as mentioned earlier. Ultimately, the high self-healing efficiency observed for BC networks is attributed to enhanced uniformity in the distribution of polymer chains

for these networks thus enabling improved diffusion of HUBs within the bulk.

An additional aspect of the increase in M_C is the presence of entanglements in these networks. Polymer chains exhibit entanglements (physical crosslinks) only at sufficiently high molecular weight, typically starting at approximately 600 backbone chain atoms [31]. For this system, the total number of backbone chain atoms between permanent crosslinks is 394, 590, and 786 for a stoichiometric M_C of 6, 9, and 12 kg/mol, respectively, therefore entanglements should be present in networks with an M_C above 9 kg/mol. Given the differences between stoichiometric and measured M_C shown in Table 2, it is possible that elastically active network chains are inextricably woven owing to the disorderly RM network structures, resulting in persistent entanglements that yield high measured M_C .

Conversely, the relatively good agreement of measured to stoichiometric M_C for BC networks would indicate more uniform topologies containing elastically active network chains that are sufficiently long to exhibit entanglements. Although entanglements result in topological constraints which act to shorten diffusion length, this characteristic could aid stickers in their pursuit to re-associate; by acting as a sufficiently long steric tether, entanglements could act to support the self-diffusion characteristics of stickers by restricting the volume being swept during healing thus increasing the probability that two stickers maintain proximity to one another for an adequate duration to re-associate. Moreover, similar to the release of hydrogen bonds at elevated temperatures (see Fig. SI.6B), the strengths of chain-chain

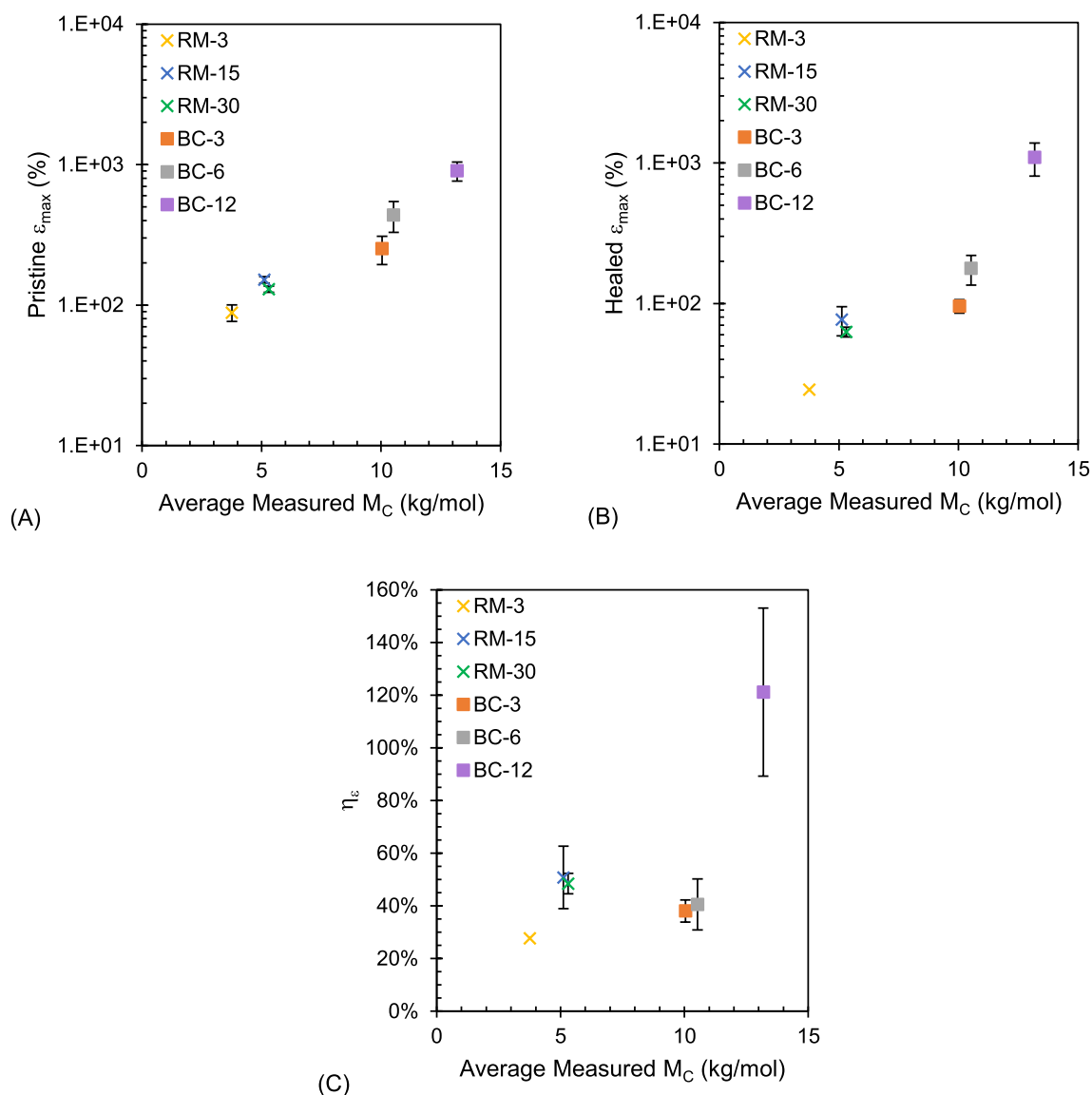


Fig. 7. Mechanical and self-healing performance are a direct consequence of the processing technique used. Resulting RM and BC networks exhibit starkly different crosslink densities which influence network topology. (A) Pristine and (B) Healed ϵ_{max} increase proportionally with measured M_C , and (C) Healing efficiency based on recovery of elongation to break.

interactions are likely softened during healing at 70 °C owing to the increase in specific volume, thus reducing the persistence of these topological constraints. The measured M_C of all BC networks are above the critical entanglement molecular weight, although BC-3 and BC-6 are very close to this threshold. The high healability of BC-12 could therefore be explained by its sufficiently high M_C which enables improved diffusion of dissociated HUBs as well as the presence of entanglements within a uniform topology.

4. Conclusions

A new poly(urea urethane) prepolymer (PUUP) was prepared and incorporated into polymer networks with thiol building blocks at multiple stoichiometric feed ratios and thus various molecular weights per elastically effective network chain (M_C). Polymer networks were catalyzed using either a photoinitiator or a base. These distinct reaction mechanisms, radical mediated (RM) or base catalyzed (BC), resulted in the formation of networks with a wide range of thermal and mechanical

properties, as well as varying degrees of self-healability. The T_g of BC networks displayed a strong negative linear trend as M_C was increased ($R^2 = 0.99$), whereas RM networks exhibited poor negative linear conformance ($R^2 = 0.84$) as M_C was increased. BC networks exhibited improved toughness in comparison to RM networks as indicated by a near 3X increase in elongation to break (ϵ_{max}) of pristine samples at the same stoichiometric M_C . The major findings of this investigation are as follows: (i) the shear storage moduli (G') of RM networks exceeded their predicted values due to the presence of higher concentrations of elastically active crosslinks (EACs) and therefore shorter elastically active network chains than BC networks, (ii) substantial differences in stoichiometric versus measured G' of 209 % (RM-15) and 493 % (RM-30) indicates that the RM polymerization mechanism resulted in disorderly network architectures, (iii) a high self-healing performance of 100 % recovery based on toughness (U_T) was exhibited by BC-12 owing to both the high measured M_C and topological uniformity of BC networks, and (iv) a 4X increase in healing efficiency based on toughness (η_U) between BC and RM formulations at the same stoichiometric M_C , as well as the

general increase in healing efficiency as measured M_c is increased, provides evidence that self-healing performance is a function of both the topological uniformity and crosslink density of prepared networks. These findings can aid in the rational design of HUB containing networks being prepared via thiol-ene chemistry, noting that the practical use of the radical mediated thiol-ene reaction appears to limit the ability of formed networks to exhibit self-healing. We suspect that this is due to the mixed-mode polymerization mechanism present in RM systems, resulting in a competition between homopolymerization of acrylates and the desirable thiol-ene reaction. We therefore emphasize the importance of reaction mechanism when preparing CANs.

CRedit authorship contribution statement

Kory Schimmelpfennig: Writing – review & editing, Writing – original draft, Visualization, Validation, Software, Methodology, Investigation, Formal analysis, Data curation, Conceptualization. **Vincent Mei:** Writing – review & editing, Visualization, Software, Methodology, Investigation, Conceptualization. **Christopher L. Lewis:** Writing – review & editing, Validation, Supervision, Resources, Project administration, Methodology, Funding acquisition, Formal analysis, Conceptualization.

Declaration of competing interest

The authors declare that they have no known competing financial interests or personal relationships that could have appeared to influence the work reported in this paper.

Funding sources

This work was supported by the United States Department of Defense [award numbers W52P1J-20-9-304 & W911NF1920158].

Appendix A. Supplementary data

Supplementary data to this article can be found online at <https://doi.org/10.1016/j.eurpolymj.2025.113736>.

Data availability

Data will be made available on request.

References

- [1] H. Baorong, L. Xiaogang, M. Xiumin, D. Cuiwei, Z. Dawei, Z. Meng, X. Weichen, L. Dongzhu and M. Fubin, "The cost of corrosion in China," *npj Materials Degradation*, vol. 1, no. 4, 2017.
- [2] V. Mei, K. Schimmelpfennig, E. Caravaca, S. Colvin, C.L. Lewis, Investigating the Structure–Property–Processing Relationship of Polycaprolactone-Based 3D Printed Self-Healing Polymer Blends, *ACS Appl. Polym. Mater.* 6 (4) (2024) 2177–2187.
- [3] K. Yu, A. Xin, H. Du, Y. Li, Q. Wang, Additive manufacturing of self-healing elastomers, *NPG Asia Mater.* 11 (1) (2019) 7.
- [4] A. Durand-Silva, K. P. Cortés-Guzmán, R. M. Johnson, S. D. Perera, S. D. Diwakara and R. A. Smaldone, "Balancing Self-Healing and Shape Stability in Dynamic Covalent Photoresins for Stereolithography 3D Printing," *ACS Macro Letters*, vol. 10, no. 4, pp. 486–491, 04 2021.
- [5] X. Li, R. Yu, Y. He, Y. Zhang, X. Yang, X. Zhao, W. Huang, Self-healing polyurethane elastomers based on a disulfide bond by digital light processing 3D printing, *ACS Macro Lett.* 8 (11) (2019) 1511–1516.
- [6] Z. Zhou, S. Chen, X. Xu, Y. Chen, L. Xu, Y. Zeng, F. Zhang, Room temperature self-healing crosslinked elastomer constructed by dynamic urea bond and hydrogen bond, *Prog. Org. Coat.* 154 (2021) 106213.
- [7] G. Binbin, J. Xinzhu, C. Xiaoteng, L. Gang, L. Yongguang, B. Jiaming, A highly stretchable and intrinsically self-healing strain sensor produced by 3D printing, *Virtual Phys. Proto.* 15 (sup1) (2020) 520–531.
- [8] B.-C.-K. Tee, C. Wang, R. Allen, Z. Bao, An electrically and mechanically self-healing composite with pressure- and flexion-sensitive properties for electronic skin applications, *Nat. Nanotechnol.* 7 (2012) 825–832.
- [9] E.F. Gomez, S.V. Wanasinghe, A.E. Flynn, O.J. Dodo, J.L. Sparks, L.A. Baldwin, C. E. Tabor, M.F. Durstock, D. Konkolewicz, C.J. Thrasher, 3D-Printed self-healing

- elastomers for modular soft robotics, *ACS Appl. Mater. Interfaces* 13 (24) (2021) 28870–28877.
- [10] S. Terry, J. Brancart, D. Lefeber, G. V. Assche and B. Vanderborght, "Self-healing soft pneumatic robots," *Science Robotics*, vol. 2, no. 9, 2017.
- [11] G.Y. Kim, S. Sung, M.P. Kim, S.C. Kim, S.-H. Lee, Y.I. Park, S.M. Noh, I.W. Cheong, J.C. Kim, Reversible polymer networks based on the dynamic hindered urea bond for scratch healing in automotive clearcoats, *Appl. Surf. Sci.* 505 (2020) 144546.
- [12] H. Ying, J. Yen, R. Wang, Y. Lai, J.-L.-A. Hsu, Y. Hu, J. Cheng, Degradable and biocompatible hydrogels bearing a hindered urea bond, *Biomater. Sci.* 5 (2017) 2398–2402.
- [13] W. Denissen, J.M. Winne, F.E. Du Prez, Vitrimers: permanent organic networks with glass-like fluidity, *Chem. Sci.* 7 (2016) 30–38.
- [14] Y. Zhang, H. Ying, K.R. Hart, Y. Wu, A.J. Hsu, A.M. Coppola, T.A. Kim, K. Yang, N. R. Sottos, S.R. White, J. Cheng, Malleable and recyclable poly(urea-urethane) thermosets bearing hindered urea bonds, *Adv. Mater.* 28 (35) (2016) 7646–7651.
- [15] H. Ying, Y. Zhang, J. Cheng, Dynamic urea bond for the design of reversible and self-healing polymers, *Nat. Commun.* 5 (1) (2014) 3218.
- [16] S. Jiang, H. Huang, Mechanism-guided design of chain-growth click polymerization based on a thiol-michael reaction, *Angew. Chem. Int. Ed.* 62 (13) (2023) e202217895.
- [17] T.C. Wabnitz, J.-Q. Yu, J.B. Spencer, "Evidence that protons can be the active catalysts in Lewis acid mediated hetero-michael addition reactions," *Chem. – A European J.* 10 (2) (2004) 484–493.
- [18] T.C. Wabnitz, J.B. Spencer, A general, Brønsted acid-catalyzed hetero-michael addition of nitrogen, oxygen, and sulfur nucleophiles, *Org. Lett.* 5 (12) (2003) 2141–2144.
- [19] D. M. Beaupre and R. G. Weiss, "Thiol- and Disulfide-Based Stimulus-Responsive Soft Materials and Self-Assembling Systems," *Molecules*, vol. 26, no. 11, 2021.
- [20] C.E. Hoyle, C.N. Bowman, Thiol-ene click chemistry, *Angew. Chem. Int. Ed Engl.* 49 (9) (Feb 2010) 1540–1573.
- [21] J.W. Chan, C.E. Hoyle, A.B. Lowe, M. Bowman, Nucleophile-initiated thiol-michael reactions: Effect of organocatalyst, thiol, and ene, *Macromolecules* 43 (15) (2010) 6381–6388.
- [22] Z. Zhou, S. Chen, W. Li, J. He, C. Yu, F. Zhang, Mechanically stable dynamic urea bond-based crosslinked polymer blend with tunable self-healable and physical properties, *Macromol. Mater. Eng.* 306 (1) (2021) 2000527.
- [23] S.J. Garcia, Effect of polymer architecture on the intrinsic self-healing character of polymers, *Eur. Polym. J.* 53 (2014) 118–125.
- [24] ChemEurope, "Isophorone diisocyanate," [Online]. Available: https://www.chemieurope.com/en/encyclopedia/Isophorone_diisocyanate.html.
- [25] R.H. Aguirresarobe, S. Nevejans, B. Reck, L. Irusta, H. Sardon, J.M. Asua, N. Ballard, Healable and self-healing polyurethanes using dynamic chemistry, *Prog. Polym. Sci.* 114 (2021) 101362.
- [26] P. Phoungtawee, D. Crespy, Shining a new light on the structure of polyurea/polyurethane materials, *Polym. Chem.* 12 (2021) 3893–3899.
- [27] G.Y. Kim, S. Sung, M.P. Kim, S.C. Kim, S.-H. Lee, Y.I. Park, S.M. Noh, I.W. Cheong, J.C. Kim, Reversible polymer networks based on the dynamic hindered urea bond for scratch healing in automotive clearcoats, *Appl. Surf. Sci.* 505 (March 2020).
- [28] D.G. Lee, S. Sung, D.G. Oh, Y.I. Park, S.-H. Lee, J.C. Kim, S.M. Noh, H.W. Jung, Application of polycarbonate diol containing hindered urea to polyurethane-based clearcoats for tuning of scratch-healing properties, *J. Coat. Technol. Res.* 17 (February 2020) 963–976.
- [29] T.G. Fox, S. Loshaek, Influence of molecular weight and degree of crosslinking on the specific volume and glass temperature of polymers, *J. Polym. Sci.* 15 (80) (1955) 371–390.
- [30] K. Bandzierz, L. Reuvekamp, J. Dryzek, W. Dierkes, A. Blume and D. Bielski, "Influence of Network Structure on Glass Transition Temperature of Elastomers," *Materials (Basel)*, vol. 9, no. 7, 2016.
- [31] L.H. Sperling, Introduction to physical polymer science, Wiley, 2005.
- [32] L.W. Hill, Calculation of crosslink density in short chain networks, *Prog. Org. Coat.* 31 (3) (1997) 235–243.
- [33] M. Doi, S.F. Edwards, The theory of polymer dynamics, Clarendon Press, 1988.
- [34] Y. Akagi, J.P. Gong, U.-I. Chung, T. Sakai, Transition between phantom and affine network model observed in polymer gels with controlled network structure, *Macromolecules* 46 (3) (2013) 1035–1040.
- [35] N.J. Bongiardina, J. Sinha, C.N. Bowman, Flory–huggins parameters for thiol-ene networks using hansen solubility parameters, *Macromolecules* 54 (24) (2021) 11439–11448.
- [36] N.R. Richbourg, M. Wancura, A.E. Gilchrist, S. Toubbeh, B.A.C. Harley, E. Cosgriff-Hernandez, N.A. Peppas, Precise control of synthetic hydrogel network structure via linear, independent synthesis-swelling relationships, *Sci. Adv.* 7 (7) (2021) p. eabe3245.
- [37] K. Dušek, M. Dušková-Smrčková, Network structure formation during crosslinking of organic coating systems, *Prog. Polym. Sci.* 25 (9) (2000) 1215–1260.
- [38] H.R. Kricheldorf, The role of self-dilution in step-growth polymerizations, *Macromol. Rapid Commun.* 29 (21) (2008) 1695–1704.
- [39] P.J. Flory, Statistical thermodynamics of random networks, *Proceed. The Royal Soc. A* 351 (1666) (1976) 351–380.
- [40] M. Uygün, M.A. Tasdelen, Y. Yagci, Influence of type of initiation on thiol-ene "Click" chemistry, *Macromol. Chem. Phys.* 211 (1) (2010) 103–110.
- [41] Q. Li, H. Zhou, C.E. Hoyle, "The effect of thiol and ene structures on thiol-ene networks: Photopolymerization, physical, mechanical and optical properties", *Polymer* 50 (10) (2009) 2237–2245.
- [42] A.Y. Rulev, Aza-michael reaction: A decade later – is the research over? *Eur. J. Org. Chem.* 26 (26) (2023) e202300451.

- [43] R.B. Roseli, A.B. Keto, E.H. Krenske, Mechanistic aspects of thiol additions to Michael acceptors: Insights from computations, *WIREs Comput. Mol. Sci.* 13 (2) (2023) e1636.
- [44] M. R. A.N. Semenov, Thermoreversible gelation in solutions of associating polymers. 2. linear dynamics, *Macromolecules* 31 (4) (1988) 1386–1397.
- [45] M. R. & A. N. Semenov, "Dynamics of Entangled Solutions of Associating Polymers," *Macromolecules*, vol. 34, no. 4, 2001.
- [46] R. P. Wool and K. M. O'Connor, "A theory crack healing in polymers," *Journal of Applied Physics*, vol. 52, no. 10, pp. 5953-5963, 10 1981.
- [47] T. Patel, M.P. Kim, J. Park, T.H. Lee, P. Nallepalli, S.M. Noh, H.W. Jung, H. Ko, J. K. Oh, Self-healable reprocessable triboelectric nanogenerators fabricated with vitrimeric poly(hindered urea) networks, *ACS Nano* 14 (9) (2020) 11442–11451.
- [48] K. Choi, H.P. Hong, K. Kim, J. Kang, H.J. Park, J. Kim, Y. Kim, M.J. Ka, S.W. Hong, Highly flexible and transparent self-healing elastomer based on localized supramolecular interactions with enhanced mechanical properties and long-term storage stability, *Polym. Degrad. Stab.* 225 (July 2024).
- [49] C.L. Lewis, Y. Meng, M. Anthamatten, Well-Defined shape-memory networks with high elastic energy capacity, *Macromolecules* 48 (14) (2015) 4918–4926.